RESEARCH ARTICLE

Convective rain cell characteristics and scaling in climate projections for Germany

Christopher Purr[1] | Erwan Brisson[1,2] | Bodo Ahrens[1]

[1]Institute for Atmospheric and Environmental Sciences, Goethe University Frankfurt, Frankfurt, Germany

[2]Centre National de Recherches Météorologiques, Toulouse, France

Correspondence
Christopher Purr, Institute for Atmospheric and Environmental Sciences, Goethe University Frankfurt, Altenhöferallee 1, Frankfurt 60438, Germany.
Email: purr@iau.uni-frankfurt.de

Abstract

Extreme convective precipitation is expected to increase with global warming. However, the rate of increase and the understanding of contributing processes remain highly uncertain. We investigated characteristics of convective rain cells like area, intensity, and lifetime as simulated by a convection-permitting climate model in the area of Germany under historical (1976–2005) and future (end-of-century, RCP8.5 scenario) conditions. To this end, a tracking algorithm was applied to 5-min precipitation output. While the number of convective cells is virtually similar under historical and future conditions, there are more intense and larger cells in the future. This yields an increase in hourly precipitation extremes, although mean precipitation decreases. The relative change in the frequency distributions of area, intensity, and precipitation sum per cell is highest for the most extreme percentiles, suggesting that extreme events intensify the most. Furthermore, we investigated the temperature and moisture scaling of cell characteristics. The temperature scaling drops off at high temperatures, with a shift in drop-off towards higher temperatures in the future, allowing for higher peak values. In contrast, dew point temperature scaling shows consistent rates across the whole dew point range. Cell characteristics scale at varying rates, either below (mean intensity), at about (maximum intensity and area), or above (precipitation sum) the Clausius–Clapeyron rate. Thus, the widely investigated extreme precipitation scaling at fixed locations is a complex product of the scaling of different cell characteristics. The dew point scaling rates and absolute values of the scaling curves in historical and future conditions are closest for the highest percentiles. Therefore, near-surface humidity provides a good predictor for the upper limit of for example, maximum intensity and total precipitation of individual convective cells. However, the frequency distribution of the number of cells depending on dew point temperature changes in the future, preventing statistical inference of extreme precipitation from near-surface humidity.

KEYWORDS

Clausius–Clapeyron scaling, convection-permitting simulation, convective storms, COSMO-CLM, precipitation, tracking

1 | INTRODUCTION

The question of how extreme precipitation will change in the future due to climate change is of high relevance due to the potentially severe hazards accompanying it. While daily precipitation extremes are projected to increase close to the Clausius–Clapeyron (CC) rate of ca. 7%/K on average in mid-latitudes, the change of precipitation extremes at regional level and on shorter time scales (e.g., hourly) is still uncertain (Zhang *et al.*, 2017).

Observational studies show that the temperature scaling of extreme precipitation can divert from the CC rate on sub-daily timescales (Lenderink and van Meijgaard, 2008), especially in the case of convective precipitation (Berg *et al.*, 2013). Furthermore, Schroeer and Kirchengast (2018) showed that the scaling can vary considerably at small spatial scales and depending on the season.

Since hourly precipitation extremes are primarily caused by convective precipitation in mid-latitudes, it is necessary to use models that can simulate deep convection explicitly, so-called convection-permitting climate models (CPMs). CPMs substantially improve the representation of convective precipitation, especially in terms of extreme precipitation, in contrast to coarser models, parameterizing deep convection (Prein *et al.*, 2015; Brisson *et al.*, 2016). Convection-permitting simulations agree on an increase in extreme hourly precipitation with global warming showing the highest increases for the highest percentiles (Knist *et al.*, 2018).

A common way of investigating extreme precipitation in CPMs is calculating the temperature scaling of precipitation extremes. The temperature scaling on the hourly scale found in CPM studies varies between values slightly below (Fosser *et al.*, 2017) or above the CC rate (Kendon *et al.*, 2014; Knist *et al.*, 2018). What is common among these studies is that the scaling curves keep their characteristic shape but are shifted towards higher peak values at high temperatures in future conditions (Prein *et al.*, 2017a). This suggests that atmospheric conditions with sufficient humidity are present at higher temperatures in the future.

Varying scaling rates in observations and shifting scaling curves in CPMs indicate that the dynamics of deep convection and changes in the large-scale environment have a strong influence on the scaling rate and that the temperature scaling of extreme hourly precipitation under current climate conditions cannot be used to infer how convective events might react to climate change.

The rationale behind the procedure of relating extreme precipitation to near-surface temperature is that near-surface temperature provides a proxy for absolute humidity if relative humidity remains unchanged.

However, the severity and structure of deep convective storms are determined by at least two additional ingredients besides near-surface moisture: static instability, as measured, for example, by convective available potential energy (CAPE), and wind shear (Weisman and Klemp, 1982). When coarse regional or global climate models (grid spacing larger than 4 km) are used to investigate how severe convection might change in a warmer climate, a combination of these three parameters is usually used to calculate changes in the frequency of thermodynamic environments favourable for convection (e.g., Seeley and Romps, 2015). Púčik *et al.* (2017) found an increase in storm favouring environments in Europe based on an ensemble of 14 regional climate models.

Solid understanding of the changes in deep convection and the processes involved can strengthen the reliability and plausibility of results. Therefore, we apply a tracking algorithm to 5-min precipitation output from the regional climate model COSMO-CLM to investigate convective rain cells' characteristics under historical and future conditions. Applying such a Lagrangian approach has the advantage of being able to monitor precipitating convective cells along their entire lifecycle. Observational studies based on weather radars show that convective cells increase in area and intensity with temperature in central Europe (Moseley *et al.*, 2013; Lochbihler *et al.*, 2017; Purr *et al.*, 2019), whereas no area increase and generally lower scaling rates were found in Mediterranean and semi-arid climate (Peleg *et al.*, 2018). Prein *et al.* (2017b) investigated the characteristics of Mesoscale Convective Systems in the USA by applying a tracking algorithm to hourly precipitation data from a CPM. They found an increase in the storm size and storm intensity for future conditions using a pseudo-global warming approach. Rasmussen *et al.* (2020) found an increase in intense convective precipitation events and a decrease in moderate events for North America at the end of the century. They used the WRF-model in a pseudo global warming setup. They attributed these changes to increases in both CAPE and convective inhibition (CIN).

This study compares cell characteristics and their dependence on near-surface temperature and humidity in two 30-year periods, covering historical (1976–2005) and future (2071–2100) conditions. We relate the scaling of cell characteristics to the scaling of precipitation at fixed locations and discuss the influence of static stability and wind shear on the scaling rates.

In Section 2, we describe the simulations that were performed and the tracking algorithm. The setup we use here has been shown to represent convective cell characteristics adequately in Purr *et al.* (2019). In this former study we evaluated the same model setup as used here but driven by reanalysis instead of a general circulation

model. We will refer to these evaluation results specifically by stating the model's limitations in representing the individual cell characteristics in the respective result sections. The following section describes the setup of the CPM simulations, the tracking algorithm, and the way the temperature and moisture scaling was calculated. In the result section we first show 'traditional' precipitation statistics such as change in mean precipitation and frequency distribution of hourly precipitation. Afterward, we investigate the overall frequency distributions of cell characteristics as well as their diurnal cycle and spatial distribution. Subsequently, the dependence of cell characteristics on near-surface temperature and dew point temperature is investigated. At the end, we discuss the influence of the large-scale environment described by CAPE and wind shear and potential limitations of the current study.

2 | METHODS

2.1 | COSMO simulations

The simulations analysed in this study were performed with the Consortium for Small-Scale Modelling in climate mode (COSMO-CLM) model. The COSMO-CLM model is a non-hydrostatic limited-area climate model, based on the COSMO model (Steppeler *et al*., 2003), a model designed by the Deutsche Wetterdienst (DWD) for operational weather predictions. The climate limited-area modelling (CLM) community adapted this model to perform climate projections (Böhm *et al*., 2003; Rockel *et al*., 2008). For time integration, the fifth order Runge–Kutta split-explicit time stepping scheme is used. The lower boundary fluxes are provided by the TERRA model (Doms *et al*., 2018). The radiative scheme is the Ritter and Geleyn (1992) scheme. As recommended in Brisson *et al*. (2015), we used a one-moment microphysics scheme, including graupel in the finest nest, which provides a more realistic representation of deep convective clouds. Shallow convection is parameterized using the convection scheme after Tiedtke (1989).

Two continuous 30-year long simulations were performed: 1976–2005 (named *historical* from now on) and 2071–2100 (named *RCP8.5*) at a resolution of 0.025°. The model is forced by the global climate model EC-Earth (Hazeleger *et al*., 2012), in particular realization r12i1p1 of the CMIP5 ensemble, in a one-way nesting setup with an intermediate COSMO-CLM nest which has a resolution of 0.22°. The RCP8.5 emission scenario was used for the future simulation. The model domain covers an area in central Europe (Figure 1) and comprises 368 × 306 grid points.
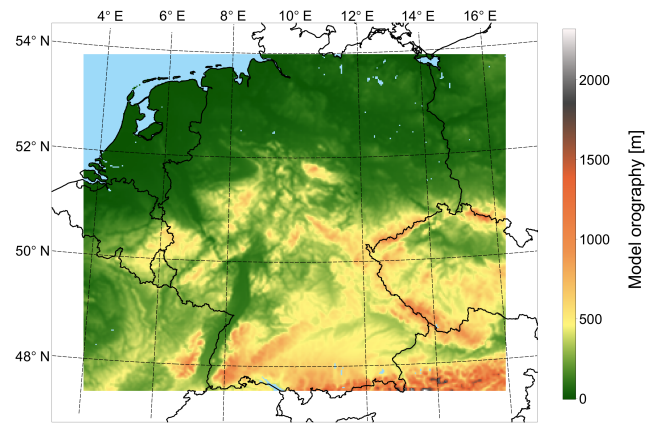

FIGURE 1 Model domain of the 0.025° simulation. Colours indicate the model orography in the evaluation region. The non-coloured margin is the relaxation zone, which is not used for evaluation [Colour figure can be viewed at wileyonlinelibrary.com]

2.2 | Tracking algorithm

We use a tracking algorithm to obtain convective cell characteristics from model simulations. A detailed description of the tracking algorithm can be found in Purr *et al*. (2019). In summary, the tracking algorithm consists of three major steps:

1. Contiguous precipitation areas with precipitation intensity above a threshold of 8.5 mm/hr (within 5 min), potential convective objects, are identified in the current and the subsequent time step. The minimum cell area is set to 4 grid points.
2. Wind information is used to predict the position of the cell at the subsequent time step. To this end, a 'cone of detection' is set up for each pixel of every cell in the current time step. If a new cell is present in the cone, a probability value is assigned to the origin pixel of the cone, which links this pixel to the new cell.
3. The probability values of all pixels are summed up for each cell. If a single cell is present in the cone, the corresponding objects from the current and the subsequent time step are connected. If multiple cells are present, the current cell is associated with the cell with the highest probability in the subsequent time step.

Cells are considered for analysis only if they are traceable for at least three time steps. It should be noted that cell mergers and splits are not accounted for. If two cells merge, the cell track with the higher probability of cell association is continued. The other track is regarded as an individual track in itself. The same applies to cells that split. The characteristics that are extracted by the

algorithm for each cell are: (1) lifetime; (2) mean intensity, that is, the temporal and spatial mean over the entire lifetime; (3) maximum intensity, that is, the highest grid-point intensity during the entire lifetime; (4) maximum area, defined as the maximum instantaneous area over the entire lifetime; (5) precipitation sum, that is, the total spatial and temporal precipitation sum over the entire lifetime; and (6) mean speed, defined as the temporal mean speed of the cells' centre of mass.

2.3 | Temperature- and moisture-scaling methods

The temperature and moisture scaling of cell characteristics are investigated by assigning 2 m-temperature and 2 m-dew point temperature to each cell. We use daily mean values of temperature and dew point temperature from the driving, intermediate nest. For each cell, the respective conditions at the start location of the cell are used.

Cells are sorted into bins of 1°C width for both temperature and dew point. For each bin, the 95th and 99th percentiles of the investigated cell characteristics are computed. The scaling rates s_i are computed as the fractional change of the respective quantity (e.g., precipitation sum, maximum intensity, etc.) P from bin i to $i + 1$ as: $s_i = ln\frac{P_{i+1}}{P_i}/(T_{i+1} - T_i)$ where T denotes temperature or dew point temperature for temperature and dew point temperature scaling, respectively.

3 | RESULTS AND DISCUSSION

The following section starts by describing the simulations' general precipitation statistics, and putting them into context with other regional climate simulations. Afterward, the frequency distributions, spatial distribution, and diurnal cycle of convective cell characteristics are analysed in Section 3.2. The scaling of these characteristics with temperature and dew point temperature is investigated in Section 3.3, followed by a description of the influence of CAPE and wind shear on these scalings.

3.1 | Mean and extreme precipitation

Mean summer precipitation (Apr–Sep) is reduced by 15% in the future period compared to historical conditions on domain average (Figure 2). The mean temperature change signal in the simulation is +3.4 K. Both values are within the range of the EURO-CORDEX ensemble projections (Jacob *et al.*, 2014). The mean dew point
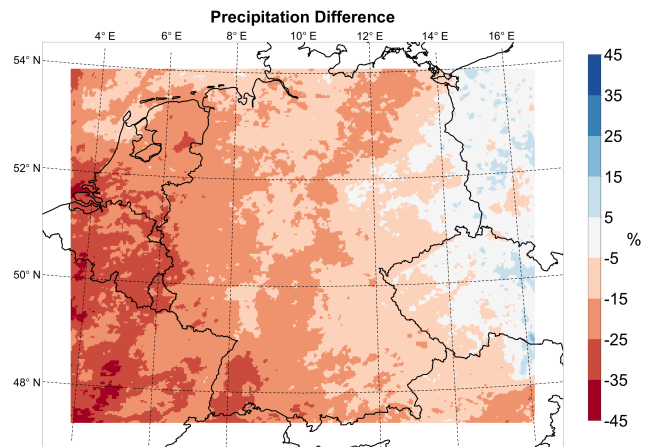

FIGURE 2 Relative change in mean summer (APR-SEP) precipitation from historical to RCP8.5 [Colour figure can be viewed at wileyonlinelibrary.com]
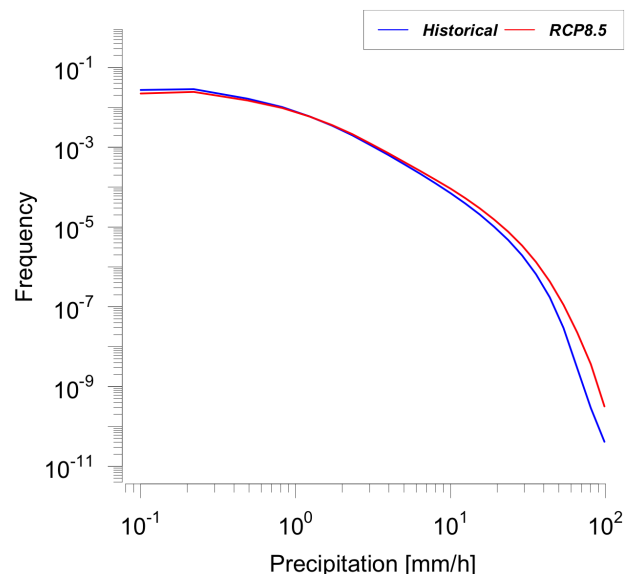

FIGURE 3 Frequency distribution of hourly precipitation intensity in historical (blue) and RCP8.5 (red) [Colour figure can be viewed at wileyonlinelibrary.com]

temperature change is +3.0 K. The reduction of precipitation is strongest in the Southwest of the domain covering northeastern France and the Netherlands. In the eastern part of the domain, there is an increase in precipitation.

Despite the decrease in mean precipitation, the frequency of hourly precipitation intensities above 5 mm/hr increases. The relative change is highest for the highest percentiles (Figure 3). Accordingly, mean convective precipitation (defined as spatial and temporal mean of precipitation classified by the tracking algorithm) increases from 0.25 to 0.29 mm/day, whereas non-classified precipitation decreases from 1.34 to 1.05 mm/day. This

translates to an increase in the fraction of convective to total precipitation from 15.8 to 21.8%.

3.2 | Cell characteristics

In this subsection, we investigate the frequency distributions of cell characteristics as well as the diurnal cycle and the spatial distribution of convective cells. The number of cells remains approximately constant. In the future simulation, ca. 5×10^5 cells are detected, which is a decrease of only 0.4% compared to the historical simulation. The frequency distribution of cell lifetime does not change either (Figure 4a). There is a decrease in frequency towards longer lifetimes in both simulations. The median and 99th percentile of cell lifetime are 35 and 255 min respectively in both *historical* and *RCP8.5*. There is a shift towards higher mean (Figure 4b) and maximum intensity. Furthermore, maximum cell area is increasing (Figure 4c). The increase in mean intensity and area

results in an increase in total precipitation sum per cell (Figure 4d).

The relative increase is strongest for the highest percentiles for all of these characteristics (mean and maximum intensity, area, and precipitation sum). However, caution should be taken when interpreting results related to the most severe cells since it has been shown that the precipitation intensity is underestimated by the model especially for long-lasting, organized convection (Purr *et al.*, 2019). Table 1 summarizes the relative changes. The trend scaling (relative changes divided by the mean temperature change signal, Zhang *et al.*, 2017) is slightly above the CC rate for the highest percentiles of precipitation sum and maximum area and below the CC rate for mean and maximum intensity.

The mean speed of convective cells increases in the future by 9%. The increase is approximately constant for all percentiles showing the highest value for the 99th percentile with +11%. Interestingly, the mean large-scale wind speed in the mid-troposphere, provided by the
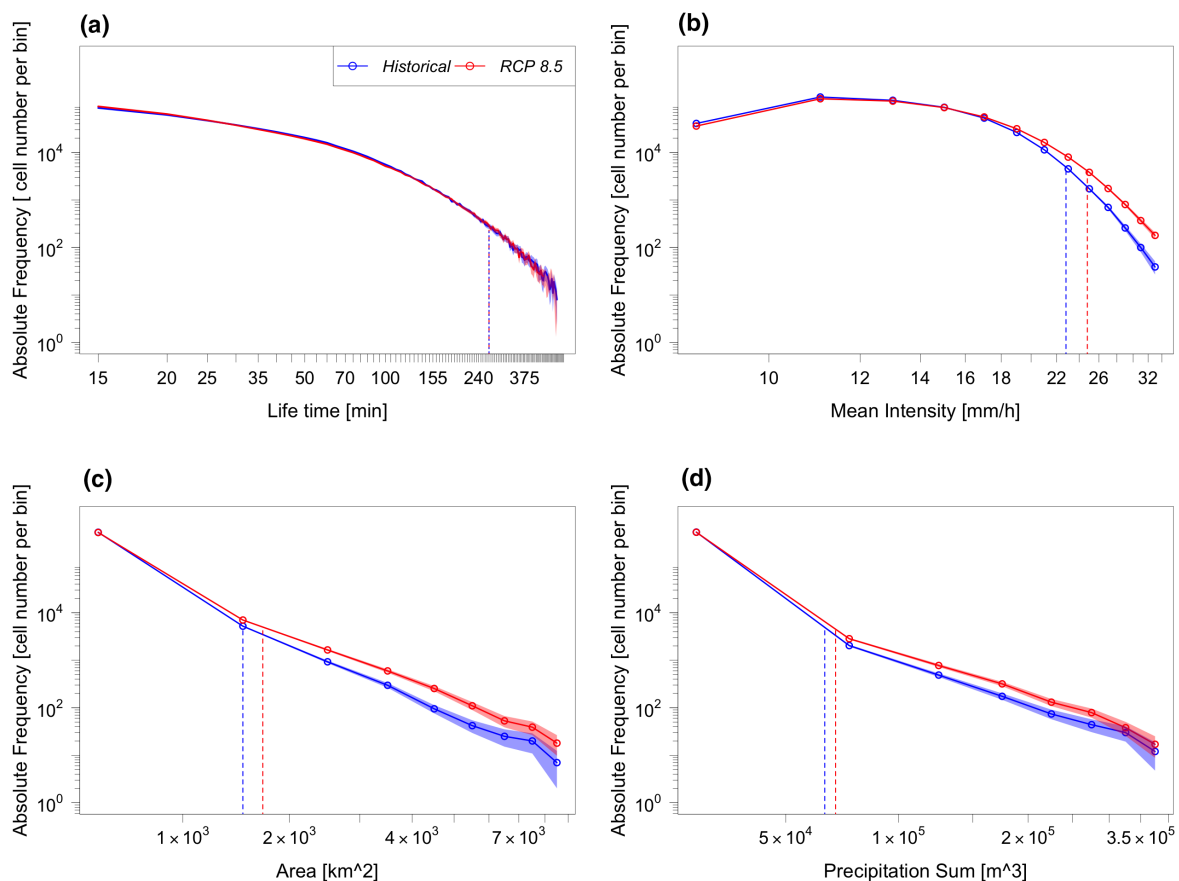

FIGURE 4 Frequency distribution of cell characteristics in the historical (blue) and RCP8.5 (red) simulations: (a) lifetime, (b) mean intensity, (c) maximum area, (d) precipitation sum. Shaded areas denote the 95% confidence interval obtained from 1,000 bootstrap samples of all cells. Dashed, vertical lines denote the 99th percentiles. Circles show the midpoints of bins [Colour figure can be viewed at wileyonlinelibrary.com]

TABLE 1 Relative changes (from historical to RCP8.5) in the frequency of cell characteristics

Change in %	Lifetime	Max. area	Precipitation sum	Mean intensity	Max intensity	Mean speed
Mean	−2.1	+13.4	+18.3	+3.3	+8.3	+9.0
Median	0.0	+9.1	+3.2	+2.4	+5.8	+7.9
P95	0.0	+16.9	+16.9	+6.4	+12.6	+10.0
P99	0.0	+27.9	+27.0	+9.3	+15.8	+11.0
P99.9	+1.1	+32.0	+30.6	+11.3	+19.1	+13.4
Trend scaling of P99 (%/K)	0.0	+8.2	+7.9	+2.7	+4.6	+3.2
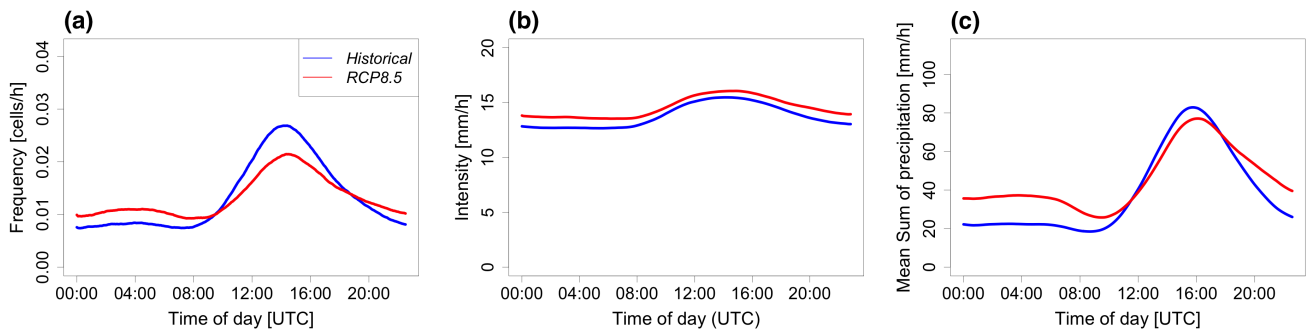
FIGURE 5 Diurnal cycle of (a) number of cells, (b) mean intensity per cell, and (c) mean sum of convective precipitation [Colour figure can be viewed at wileyonlinelibrary.com]

daily-mean wind speed in the 850, 700, and 500 hPa height levels of the driving intermediate simulation does not change accordingly. The overall mean changes in daily mean wind speed are between −0.7 and −3.9% for the 500 and 850 hPa levels. The changes in the 99th percentile of daily mean wind speed are within ±1% for all three levels. However, when only considering the large-scale wind speed in the presence of convective cells, there is an increase between 4.5 (850 hPa) and 7.7% (500 hPa) in mean wind speed.

3.2.1 | Diurnal cycle

Deep convection has a pronounced maximum in the afternoon in mid-latitudes over land caused by solar insulation, which acts to destabilize the boundary layer. The model is capable of reproducing the timing of this maximum with a delay of about 40 min compared to observations (Purr *et al*., 2019). This characteristic convective maximum is damped in the future, whereas the number of convective cells increases during the night and morning hours (Figure 5a). In contrast to the number of cells, the mean intensity per cell increases throughout the whole diurnal cycle in the future compared to present

conditions (Figure 5b). This increase in precipitation per cell compensates for the drop in the number of cells resulting in only a slight decrease in total convective precipitation in the afternoon and an increase during the nighttime and early morning hours (Figure 5c). These results are in line with the findings of Meredith *et al*. (2019), who report a shift in the diurnal cycle of extreme precipitation from afternoon to early morning hours for future conditions under RCP8.5 using COSMO-CLM-simulations driven by MPI-ESM.

The increase in cell speed reported in the previous subsection is present during the whole diurnal cycle but is more pronounced at the time of increased convective activity. While the mean speed of cells initiated between 00:00 UTC and 09:00 UTC increases from 3.8 to 4.0 m/s (i.e., 5.2%), this value increases from 3.2 to 3.5 m/s (i.e., 8.8%) for cells initiated between 09:00 UTC and 18:00 UTC. This increase during the daytime is mainly caused by fewer slow-moving cells. Stratifying cells as slow-moving (< 3.3 m/s) and fast-moving (> 3.3 m/s) shows that the number of slow-moving cells decreases by 24%, whereas the number of fast-moving cells decreases by 5% during the daytime. This decrease in slow-moving cells is not present during nighttime, where slow-moving cells increase by 22%, and fast-moving cells increase by 34%.

3.2.2 | Spatial distribution

The spatial distribution of convective cells is tightly coupled to the orography in Germany since mountains can initiate deep convection through various processes. The regions of highest convective activity in Germany are the alpine and pre-alpine area as well as the Black forest with values up to four times as high as in the flatlands of Northern Germany (Figure 6a). The model is capable of reproducing the observed spatial distribution of convective cells in Germany with a tendency to overestimate convective activity in the mountains and to underestimate it slightly in the lowlands (Purr *et al.*, 2019).

The total number of cells stays approximately constant in the future, but the change in cell number varies considerably in space (Figure 6b). In South-West Germany, the number of convective cells decreases while in the North-East increases prevail. However, these changes are not uniform, and changes between increases and decreases occur at small spatial scales of about 10–100 km. This pattern is not related to orography and likely caused by internal variability of the convective cells. Mean intensity increases throughout the domain. The sum of convective precipitation, which can be derived as cell number times mean intensity, therefore, shows a pattern similar to the number of convective cells (Figure 6c).

3.3 | Temperature and moisture scaling

In this subsection, we investigate the scaling of cell properties with temperature and dew point temperature as a measure for absolute humidity. The highest percentiles of cell area, mean intensity, maximum intensity, and precipitation sum increase with temperature. All of these characteristics follow a qualitatively similar increase up to a specific temperature. Above this temperature, the scaling
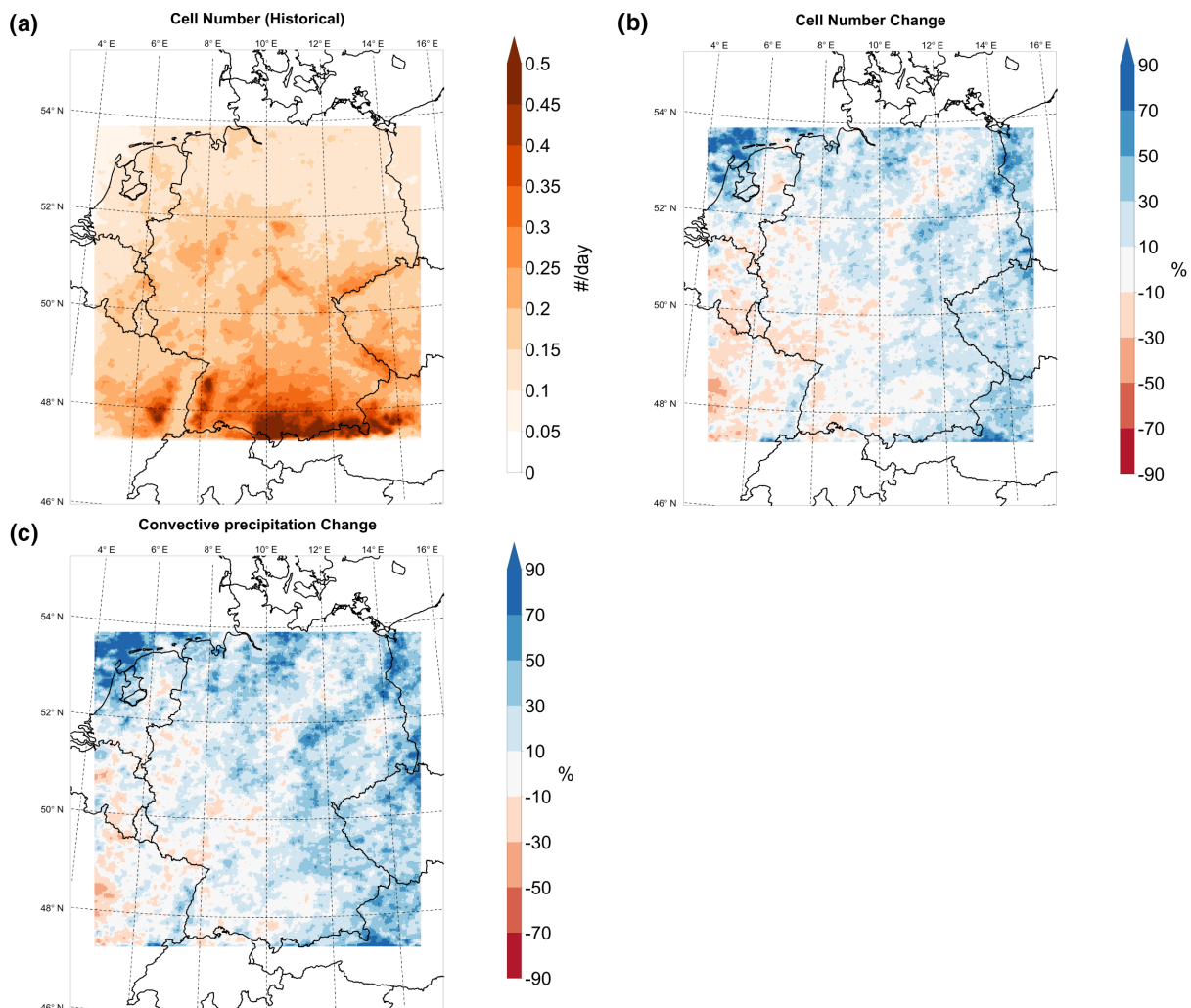

FIGURE 6 Spatial distribution of (a) cell number in the historical simulation, (b) relative change in cell number in RCP8.5, and (c) relative change in convective precipitation sum [Colour figure can be viewed at wileyonlinelibrary.com]

curves level off. In contrast to this, lifetime does not increase with temperature. The scaling rates under historical conditions are in close agreement with the temperature scaling in a simulation using a similar setup with ERA-Interim reanalysis as driving data instead of the EC-Earth model (Purr *et al.*, 2019). There are two main differences between modelled and observed scaling of cell characteristics. Firstly, the lifetime of cells does not increase with temperature in the model, whereas it does in the observations. Secondly, mean intensity levels off in the simulations whereas it increases constantly, even at high temperatures, in the observations, which can be attributed to the underestimation of intensity in long-lasting, severe cells mentioned previously.

While maximum intensity and area increase close to the CC rate at the intermediate temperature range between 10 and 20°C, mean intensity scales at considerably lower values (Figure 7a,c,e). Precipitation sum shows super CC-scaling in the intermediate temperature range and a drop-off at high temperatures (Figure 7g). The peak values for all of these characteristics are higher in the future compared to historical values and occur at higher temperatures. Thus, the scaling curves show the same characteristic shift that is well known for extreme precipitation at fixed-locations (Prein *et al.*, 2017a; Knist *et al.*, 2018) and is also found in this study (Figure S1). Furthermore, the number of cells occurring at high temperatures which have a higher potential for large precipitation sums, areas, and intensity increases (Figure 7i).

To investigate the influence of limited moisture supply at high temperatures, which has been suggested as a cause for the drop off at high temperatures, we investigate the scaling of cell properties with dew point temperature. As expected, there is no drop off at high dew point temperatures, and the scaling rates are more continuous across the whole dew point range. The maximum area increases at rates slightly above the CC rate (Figure 7b). The scaling rates for present and future conditions do not differ significantly. Also, the 99th and 95th percentile's absolute values of do not differ significantly in present and future conditions.

The scaling rates for the maximum intensity are remarkably close to the CC rate (Figure 7d). Interestingly, the 90th (not shown) and the 95th percentile values are smaller in the future compared to present conditions; the values for the 99th percentile are closer. This also implies that the scaling rates under future conditions (7.4%/K for the 99th percentile) are a little higher than under historical conditions (6.1%/K).

Like for temperature, the mean intensity scales at values lower than the CC rate (Figure 7f). Again, the absolute values for the 90th and 95th percentile under historical conditions are higher than the future values for a large part of the dew point temperature range up to 17°C. This indicates that changes in other factors (like atmospheric instability) influence the cell properties in the future. The precipitation sum scales at values of about 14%/K close to twice the CC rate (Figure 7h).

More cells occur at high moisture levels in the future (Figure 7j). The increase in number at high dew point temperatures is compensated by a decrease at low dew point temperatures. While only 0.4% of all cells at present conditions occur at dew point temperatures above 18°C, in future conditions this ratio increases to 8.5% Thus, the increase in the high percentiles of the overall frequency distribution of cell properties is largely caused by more cells occurring at higher moisture levels in the future. However, when looking at the relative number of cells per dew point bin (the number of cells per dew point bin divided by the number of occurrences of the dew point bin) as indicated by the lines in Figure 7j, we see apparent differences in present and future conditions. For dew point temperatures up to 18°C, the relative number of cells is substantially lower in the future. For higher humidity levels, the relative number increases in the future while it decreases in the present. In contrast, the relative number of cells per temperature bin follows the same curve in the future with a maximum at 18°C (Figure 7i).

3.4 | Influence of static instability and wind shear

Since static instability plays a major role in determining the severity of atmospheric convection, we investigate the influence of CAPE on the moisture scaling of cell properties. In addition, the direct influence of CAPE and wind shear is investigated in Appendix S1.

From conceptual models, it can be shown that CAPE increases with warming. Specifically, peak CAPE in a continental environment which is characterized by not being in radiative-convective equilibrium scales with moisture at the CC rate (Agard and Emanuel, 2017). These findings obtained from a simplified conceptual model are also supported by more complex regional climate models. Púčik *et al.* (2017) investigated the occurrence of storm environments and found an increase in static instability under warmer conditions.

In our simulations, the highest percentiles of daily maximum CAPE increase with dew point temperature at varying rates well above the CC rate. Since high dew point values are much more abundant in the future, this leads to a strong increase in extreme CAPE values. As an example, the frequency of daily maximum CAPE exceeding 2,000 J/kg increases from 0.8 to 2.2%. The connection between the increase in CAPE and high dew point temperature is not uniform but occurs mostly at high dew
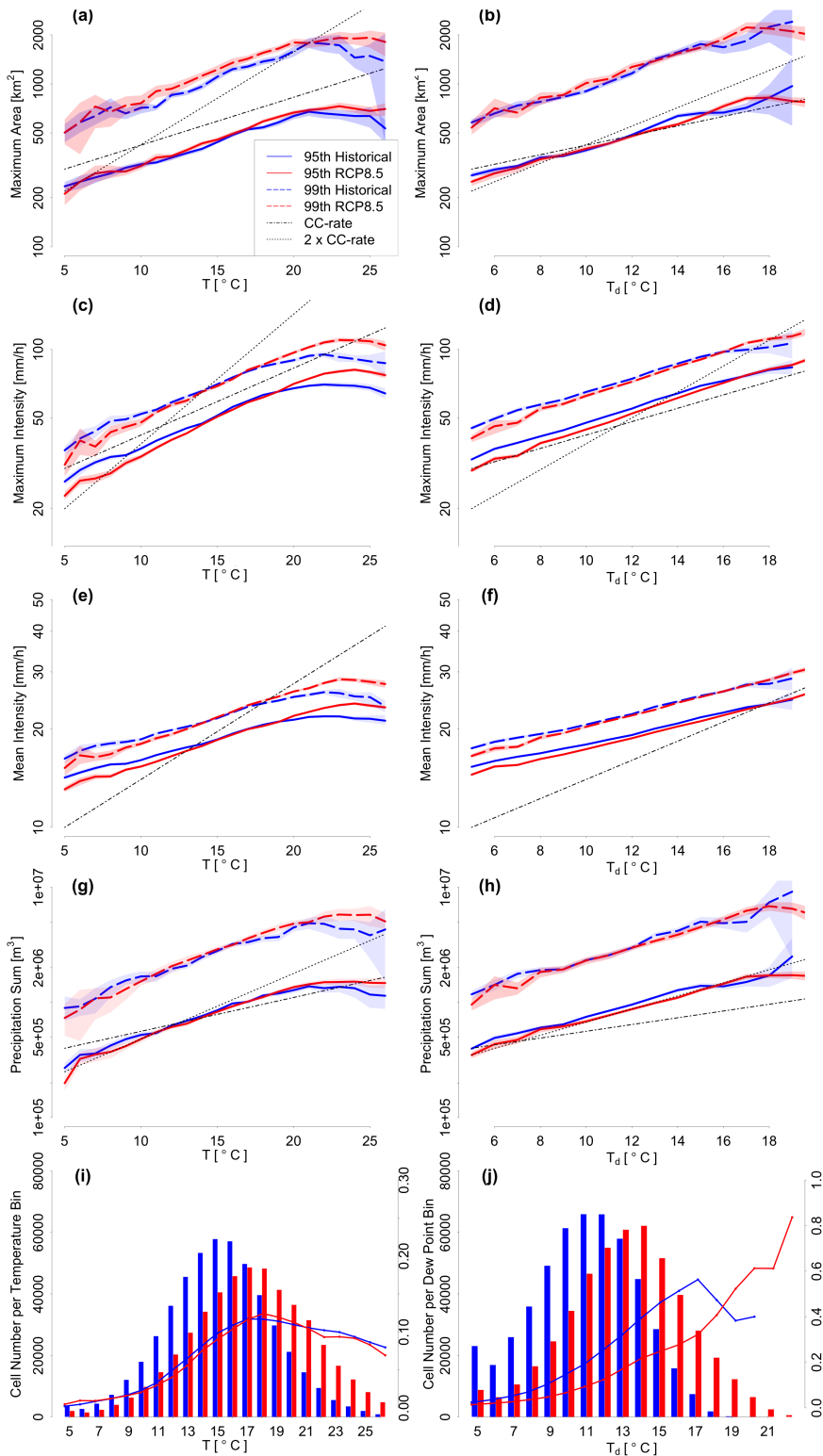
FIGURE 7 Temperature scaling (left column) and dew point temperature scaling (right column) of cell properties. (a) and (b): Maximum area; (c) and (d): Maximum intensity; (e) and (f): Mean intensity; (g) and (h): Precipitation sum. Shaded areas denote the uncertainty range caused by varying bin occupancy, obtained from bootstrapping cells in each bin. (i) and (j) show the frequency distribution of cells, where bars denote the absolute number of cells per temperature or dew point class (left y-axis) and lines denote the relative number of cells per occurrence of temperature or dew point temperature class (right y-axis) [Colour figure can be viewed at wileyonlinelibrary.com]

point levels. To investigate the effect of instability on the moisture scaling of cell properties, we stratify the convective cells according to environmental CAPE. Cells which occur at CAPE values below 200 J/kg are classified as low-CAPE cells while those above 200 J/kg are classified as high-CAPE cells. As expected, cells occurring at high

CAPE are more extreme than low-CAPE cells, as illustrated by the 99th percentile of precipitation sum for high-CAPE cells and low-CAPE cells in Figure 8a. Despite the overall increase in CAPE, the scaling rates do not change from historical to future conditions. The scaling rate of precipitation sum per cell is below the 2×CC
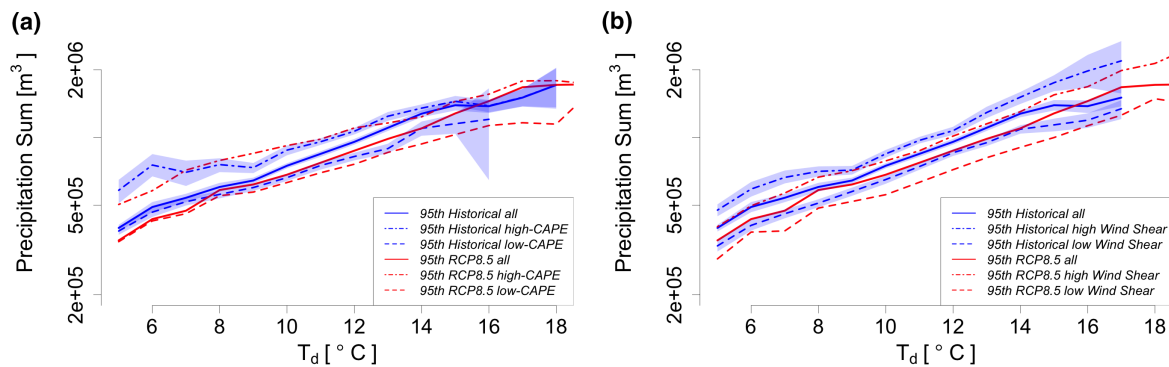
FIGURE 8   Dew point scaling of precipitation sum dependent on (a) environmental daily maximum CAPE, and (b) wind shear. Shaded areas denote the uncertainty range obtained from bootstrapping. The uncertainty range for the future period is omitted for readability [Colour figure can be viewed at wileyonlinelibrary.com]

rate found for all cells when considering only low-CAPE (historical: 5.9%/K, RCP8.5: 9.2%/K) cells or only high-CAPE cells (historical: 10.4%/K, RCP8.5: 8.8%/K). The reason for this is that more low-CAPE cells occur at low dew point temperatures and more high-CAPE cells occur at high dew point temperatures so that the overall scaling curve follows the lower values of the low-CAPE curve at low dew point temperature and shifts towards the high-CAPE curve at high dew point temperatures.

We now investigate the influence of wind shear on the scaling rates. We calculate wind shear as the difference between the wind in the 850 and 500 hPa height levels. Higher wind shear leads to higher organization of convective cells. Thus, it is not surprising that higher wind shear leads to higher precipitation sum per cell (Figure 8b). The frequency distribution of wind shear does not change in the future. In contrast to CAPE, wind shear and dew point temperature are not correlated. As a result, an equal number of low- and high-wind shear cells occur at each dew point bin. The scaling rates are identical for low-wind shear and high wind shear cells.

4 | CONCLUSIONS AND OUTLOOK

We investigated how the characteristics of convective cells might change in a climate change scenario by applying a tracking algorithm to CPM precipitation with high temporal resolution. Changes in the frequency distribution of cell characteristics show a complex picture of the response of deep convection to climate warming. While the total number of cells and the lifetime does not change significantly in the future, as simulated for the end of the 21st century under RCP8.5, there is a shift towards larger and more intense events. In combination, this leads to higher precipitation sums per cell. We showed that the increase in extreme hourly precipitation is caused by an

increase in the number of large, long-living convective cells occurring at high temperature and moisture levels.

The diurnal cycle of convective activity changes towards fewer convective cells during the afternoon maximum and more cells during the night time. In combination with the increase in mean precipitation intensity per cell this leads to up to 50% more convective precipitation during night-time and a small decrease during the afternoon maximum. The afternoon decrease in cell number is primarily caused by fewer slow-moving cells despite the fact that there is no change in the large-scale wind speed. This suggests that there is less air mass convection in the future, which would be in line with the findings of Rasmussen *et al.* (2020), who report a shift towards more extreme and less moderate events because of increased CAPE and CIN values. The increase during evening and night time could be explained by the fact that once convection is initiated, the tendency towards more intense cells implies that these cells produce stronger cold pools which can trigger new cells.

The temperature scaling curves of cell properties peak at higher values in the future, which is caused by more abundant humidity at these high temperatures, resembling the scaling curves of extreme hourly precipitation at fixed locations. In contrast to the temperature scaling, dew point scaling curves in historical and future conditions are consistent across the whole dew point range.

The CC scaling of cell area and maximum cell intensity in combination leads to super CC scaling (ca. 14%/K) of the precipitation sum per cell. As a cause for super CC scaling of extreme precipitation, a positive feedback of updraft strength with moisture supply has been discussed in the literature (Lenderink *et al.*, 2017). While this may indeed contribute to super CC scaling, we point out that the correlation of dew point temperature with CAPE may be a simple reason that can partially explain scaling above the CC rate.

The scaling curves under historical and future conditions are most similar for the highest percentiles. The

differences for the lower percentiles reflect the complex changes in the properties of convective cells related to, for example, the change in diurnal cycle. The similar dew point scaling curves for the highest percentiles of cell characteristics facilitate inference of the upper limit of convective cell properties from large scale humidity values. However, the fact that the number of convective cells per dew point bin changes both in absolute and relative terms (number of cells per occurrence of dew point bin) prevents inference of extreme precipitation at fixed locations. This is also illustrated by the differences in the dew point temperature scaling curves of extreme precipitation at fixed locations.

While one CPM simulation is not sufficient to robustly estimate the increase in extreme precipitation, the Lagrangian approach adopted here can help to understand processes related to deep convection. More projections are necessary to determine the uncertainty related to large-scale changes in the general circulation because general circulation models vary in their representation of climate change in mid-latitudes. Common deficiencies that currently limit the skill of convection-permitting climate models at the kilometre scale include the representation of cold pools as a trigger mechanism (e.g., Hirt *et al.*, 2020). Furthermore, the tracking algorithm could be enhanced to include the merging and splitting of convective cells. This would facilitate the investigation of convective organization, a topic mainly investigated in idealized simulations so far (Moseley *et al.*, 2016; Lochbihler *et al.*, 2019).

ORCID
Christopher Purr https://orcid.org/0000-0002-9376-432X
Erwan Brisson https://orcid.org/0000-0003-2558-2556
Bodo Ahrens https://orcid.org/0000-0002-6452-3180

REFERENCES
Agard, V. and Emanuel, K. (2017) Clausius–Clapeyron scaling of peak CAPE in continental convective storm environments. *Journal of the Atmospheric Sciences*, 74, 3043–3054. https://doi.org/10.1175/JAS-D-16-0352.1.

Berg, P., Moseley, C. and Haerter, J. (2013) Strong increase in convective precipitation in response to higher temperatures. *Nature Geoscience*, 6, 181–185. https://doi.org/10.1038/ngeo1731.

Böhm, U., Kücken, M., Ahrens, W., Block, A., Hauffe, D., Keuler, K., Rockel, B. and Will, A. (2003) CLM - the climate version of LM: brief description and long-term applications. *COSMO Newsletter*, 6, 225–235.

Brisson, E., Demuzere, M. and van Lipzig, N.P.M. (2015) Modelling strategies for performing convective permitting climate simulations. *Meteorologische Zeitschrift*, 25(2), 149–163. https://doi.org/10.1127/metz/2015/0598.

Brisson, E., van Weverberg, K., Demuzere, M., Devis, A., Saeed, S., Stengel, M. and van Lipzig, N.P.M. (2016) How well can a convection-permitting climate model reproduce decadal statistics of precipitation, temperature and cloud characteristics? *Climate Dynamics*, 47, 3043–3061. https://doi.org/10.1007/s00382-016-3012-z.

Doms, G.; Forstner, J.; Heis, E.; Herzog, H. J.; Raschendorfer, M.; Reinhardt, T.; Ritter, B.; Schrodin, R.; Schulz, J. P.; Vogel, G. (2018). A description of the nonhydrostatic regional COSMO model part II: physical parameterization. Technical Report.

Fosser, G., Khodayar, S. and Berg, P. (2017) Climate change in the next 30 years: what can a convection-permitting model tell us that we did not already know? *Climate Dynamics*, 48, 1987–2003. https://doi.org/10.1007/s00382-016-3186-4.

Hazeleger, W., Wang, X., Severijns, C., Ştefănescu, S., Bintanja, R., Sterl, A., Wyser, K., Semmler, T., Yang, S., van den Hurk, B., van Noije, T., van der Linden, E. and van der Wiel, K. (2012) EC-earth V2.2: description and validation of a new seamless earth system prediction model. *Climate Dynamics*, 39, 2611–2629. https://doi.org/10.1007/s00382-011-1228-5.

Hirt, M., Craig, G.C., Schäfer, S.A.K., Savre, J. and Heinze, R. (2020) Cold-pool-driven convective initiation: using causal graph analysis to determine what convection-permitting models are missing. *Quarterly Journal of the Royal Meteorological Society*, 146, 1–23. https://doi.org/10.1002/qj.3788.

Jacob, D., Petersen, J., Eggert, B., Alias, A., Christensen, O.B., Bouwer, L.M., Braun, A., Colette, A., Déqué, M., Georgievski, G., Georgopoulou, E., Gobiet, A., Menut, L., Nikulin, G., Haensler, A., Hempelmann, N., Jones, C., Keuler, K., Kovats, S., Kröner, N., Kotlarski, S., Kriegsmann, A., Martin, E., van Meijgaard, E., Moseley, C., Pfeifer, S., Preuschmann, S., Radermacher, C., Radtke, K., Rechid, D., Rounsevell, M., Samuelsson, P., Somot, S., Soussana, J.F., Teichmann, C., Valentini, R., Vautard, R., Weber, B. and Yiou, P. (2014) EURO-CORDEX: new high-resolution climate change projections for European impact research. *Regional Environmental Change*, 14, 563–578. https://doi.org/10.1007/s10113-013-0499-2.

Kendon, E.J., Roberts, N.M., Fowler, H.J., Roberts, M.J., Chan, S.C. and Senior, C.A. (2014) Heavier summer downpours with climate change revealed by weather forecast resolution model. *Nature Climate Change*, 4, 570–576. https://doi.org/10.1038/nclimate2258.

Knist, S., Goergen, K. and Simmer, C. (2018) Evaluation and projected changes of precipitation statistics in convection-permitting WRF climate simulations over Central Europe. *Climate Dynamics*, 55, 325–341. https://doi.org/10.1007/s00382-018-4147-x.

Lenderink, G., Barbero, R., Loriaux, J.M. and Fowler, H.J. (2017) Super-Clausius–Clapeyron scaling of extreme hourly convective precipitation and its relation to large-scale atmospheric conditions. *Journal of Climate*, 30, 6037–6052. https://doi.org/10.1175/JCLI-D-16-0808.1.

Lenderink, G. and van Meijgaard, E. (2008) Increase in hourly precipitation extremes beyond expectations from temperature changes. *Nature Geoscience*, 1(8), 511–514. https://doi.org/10.1038/ngeo262.

Lochbihler, K., Lenderink, G. and Siebesma, A.P. (2017) The spatial extent of rainfall events and its relation to precipitation scaling. *Geophysical Research Letters*, 44, 8629–8636. https://doi.org/10.1002/2017GL074857.

Lochbihler, K., Lenderink, G. and Siebesma, A.P. (2019) Response of extreme precipitating cell structures to atmospheric warming. *Journal of Geophysical Research: Atmospheres*, 124, 6904–6918. https://doi.org/10.1029/2018JD029954.

Meredith, E.P., Ulbrich, U. and Rust, H.W. (2019) The diurnal nature of future extreme precipitation intensification. *Geophysical Research Letters*, 46, 7680–7689. https://doi.org/10.1029/2019GL082385.

Moseley, C., Berg, P. and Haerter, J.O. (2013) Probing the precipitation life cycle by iterative rain cell tracking. *Journal of Geophysical Research – Atmospheres*, 118, 13,361–13,370. https://doi.org/10.1002/2013JD020868.

Moseley, C., Hohenegger, C., Berg, P. and Haerter, J.O. (2016) Intensification of convective extremes driven by cloud–cloud interaction. *Nature Geoscience*, 9, 748–752. https://doi.org/10.1038/ngeo2789.

Peleg, N., Marra, F., Fatichi, S., Molnar, P., Morin, E., Sharma, A. and Burlando, P. (2018) Intensification of convective rain cells at warmer temperatures observed from high-resolution weather radar data. *Journal of Hydrometeorology*, 19, 715–726. https://doi.org/10.1175/JHM-D-17-0158.1.

Prein, A., Rasmussen, R., Ikeda, K., et al. (2017a) The future intensification of hourly precipitation extremes. *Nature Climate Change*, 7, 48–52. https://doi.org/10.1038/nclimate3168.

Prein, A.F., Langhans, W., Fosser, G., Ferrone, A., Ban, N., Görgen, K., Keller, M., Tölle, M., Gutjahr, O., Feser, F., Brisson, E., Kollet, S., Schmidli, J., van Lipzig, N.P.M. and Leung, R. (2015) A review on regional convection-permitting climate modeling: demonstrations, prospects, and challenges. *Reviews of Geophysics*, 53, 323–361. https://doi.org/10.1002/2014RG000475.

Prein, A.F., Liu, C., Ikeda, K., Trier, S.B., Rasmussen, R.M., Holland, G.J. and Clark, M.P. (2017b) Increased rainfall volume from future convective storms in the US. *Nature Climate Change*, 7(12), 880–884. https://doi.org/10.1038/s41558-017-0007-7.

Púčik, T., Groenemeijer, P., Rädler, A.T., Tijssen, L., Nikulin, G., Prein, A.F., van Meijgaard, E., Fealy, R., Jacob, D. and Teichmann, C. (2017) Future changes in European severe convection environments in a regional climate model ensemble. *Journal of Climate*, 30, 6771–6794. https://doi.org/10.1175/JCLI-D-16-0777.1.

Purr, C., Brisson, E. and Ahrens, B. (2019) Convective shower characteristics simulated with the convection-permitting climate model COSMO-CLM. *Atmosphere*, 10(12), 810. https://doi.org/10.3390/atmos10120810.

Rasmussen, K.L., Prein, A.F., Rasmussen, R.M., Ikeda, K. and Liu, C. (2020) Changes in the convective population and thermodynamic environments in convection-permitting regional climate simulations over the United States. *Climate Dynamics*, 55, 383–408. https://doi.org/10.1007/s00382-017-4000-7.

Ritter, B. and Geleyn, J. (1992) A comprehensive radiation scheme for numerical weather prediction models with potential applications in climate simulations. *Monthly Weather Review*, 120, 303–325. https://doi.org/10.1175/1520-0493(1992)120<0303:ACRSFN>2.0.CO;2.

Rockel, B., Will, A. and Hense, A. (2008) The regional climate model COSMO-CLM (CCLM). *Meteorologische Zeitschrift*, 17(4), 347–348. https://doi.org/10.1127/0941-2948/2008/0309.

Schroeer, K. and Kirchengast, G. (2018) Sensitivity of extreme precipitation to temperature: the variability of scaling factors from a regional to local perspective. *Climate Dynamics*, 50, 3981–3994. https://doi.org/10.1007/s00382-017-3857-9.

Seeley, J.T. and Romps, D.M. (2015) The effect of global warming on severe thunderstorms in the United States. *Journal of Climate*, 28, 2443–2458. https://doi.org/10.1175/JCLI-D-14-00382.1.

Steppeler, J., Doms, G., Schaettler, U., Bitzer, H.W., Gassmann, A., Damrath, U. and Gregoric, G. (2003) Meso-gamma scale forecasts using the nonhydrostatic model LM. *Meteorology and Atmospheric Physics*, 82(1–4), 75–96. https://doi.org/10.1007/s00703-001-0592-9.

Tiedtke, M. (1989) A comprehensive mass flux scheme for cumulus parameterization in large-scale models. *Monthly Weather Review*, 117, 1779–1800. https://doi.org/10.1175/1520-0493(1989)117<1779:ACMFSF>2.0.CO;2.

Weisman, M.L. and Klemp, J.B. (1982) The dependence of numerically simulated convective storms on vertical wind shear and buoyancy. *Monthly Weather Review*, 110, 504–520. https://doi.org/10.1175/1520-0493(1982)110<0504:TDONSC>2.0.CO;2.

Zhang, X., Zwiers, F., Li, G., Wan, H. and Cannon, A.J. (2017) Complexity in estimating past and future extreme short-duration rainfall. *Nature Geoscience*, 10, 255–259. https://doi.org/10.1038/ngeo2911.

SUPPORTING INFORMATION

Additional supporting information may be found online in the Supporting Information section at the end of this article.